Hindawi
Shock and Vibration
Volume 2019, Article ID 2190462, 17 pages
https://doi.org/10.1155/2019/2190462

Research Article

Mechanism Study and Reduction of Minivan Interior Booming Noise during Acceleration

Yudong Wu,[1] **Renxian Li**,[1] **Weiping Ding**,[1,2] **Jan Croes**,[3] **and Mingliang Yang**[1]

[1]*School of Mechanical Engineering, Southwest Jiaotong University, Chengdu 610000, China*
[2]*Engineering Research Center of Advanced Driving Energy-Saving Technology, Ministry of Education, Chengdu 610000, China*
[3]*Department of Mechanical Engineering, KU Leuven, Heverlee, 3001 Leuven, Belgium*

Correspondence should be addressed to Weiping Ding; dwp@home.swjtu.edu.cn

Received 14 April 2019; Revised 13 June 2019; Accepted 11 August 2019; Published 29 August 2019

Academic Editor: Lutz Auersch

Interior booming noise during acceleration has been one of the most significant NVH problems for minivans. However, the generation mechanism of the interior booming noise remains unclear, so the access to reduce the booming noise is blocked. To solve the booming noise problem, a Source-Path-Receiver-Model-based approach is established to study the generation mechanism of the booming noise. Based on the generation mechanism, several modifications are proposed to reduce the minivan booming noise. In the established approach, the transfer path of the booming noise energy is figured out by the vehicle body and cavity experimental TPA, rear suspension dynamic analysis, and drivetrain torsional vibration analysis. Meanwhile, the vibroacoustic energy in the transfer processes is analyzed quantitatively. The identified generation mechanism is validated by the comparison of the test results of minivan interior noise and the simulation results from the established approach. During the minivan acceleration, the 5^{th} torsional vibration mode (50.5 Hz) of the driveline is excited by the engine torsional vibration around 1500 r/min. Then, the driveline torsional resonance energy is transferred to the body and cavity through the rear suspension and finally leads to the interior booming noise. Based on the validated mechanism, several modifications are proposed to reduce the frequency response function of the driveline, the rear suspension, and the vehicle body around 50 Hz. With these modifications applied to the minivan, it is shown in the experimental results that the interior booming noise is reduced around 1500 r/min engine speed during acceleration. The mechanism study provides effective assistance with minivan interior booming noise reduction and the study approach also could be extended to explore the mechanism of other complex interior noise problems in automobiles.

1. Introduction

Automotive ownership in Asia has been continuously and rapidly rising during recent years [1, 2], but what followed are some serious problems of urban space and energy resources, so a kind of small and low-energy consumption automobile is strongly demanded; therefore, minivan is becoming more and more popular due to its advantages in small size, good fuel efficiency, and multipurpose [3, 4]. As minivans are more and more frequently used in carrying passengers, customers are paying more attention on the NVH performance and some NVH problems come out in minivans. One of the most significant is the interior booming noise during acceleration. This issue even turns to be more acute in East Asia, because booming noise is more annoying for the East Asians [5–7].

Over the past 35 years, many researchers have attempted to control the automotive internal booming noise. Much of this work has been focused on vehicle body. The internal sound field in the enclosed cavity is shown to be significantly affected by the acoustic characteristics of the cavity, the structural vibration of the compartment wall panels and the coupling of these two dynamic systems [8–17]. Since the amount of absorptive material required to control low-frequency noise can be prohibitively large, the most practical solution to the problem would seem to be modification of the vehicle structure. However, with the increase of engine power and the lightweight of vehicle body, the potential of

structural modification to control the internal booming noise is becoming smaller. Especially in the real industrial world, only small changes on the vehicle body panels are allowed due to the mass production, so it is not enough to restrain the internal booming noise. Therefore, other possible effective methods in internal booming noise reduction have been sought. People start to turn to the vibration sources and the paths through which vibration energy can penetrate the cavity. But the automobile chassis is a very complex system as it contains a variety of mechanical components and excitations [18–24], and what's more, early in the minivan development process, manufacturers did not pay enough attention on this problem, so the generation mechanism of interior booming noise remains unclear. This is also the reason why various methods have been tried in solving the booming noise problem by minivan manufacturers, but no satisfactory effect is reached.

In this study, the common phenomenon of the interior booming noise in minivans during acceleration is introduced based on experimental results. An approach based on the "Source-Path-Receiver" model [25, 26] is established to study the interior booming noise. The generation mechanism of the booming noise is identified by the proposed approach and validated by the comparison of interior noise test and quantitative simulation results. Based on the validated mechanism, several noise reduction modifications are proposed and applied to the minivan subsystems.

2. Problem Description

The interior booming noise problem occurred while minivans were accelerating on a straight flat road. When the engine was working in the range of low rotational speed (under 2000 r/min), the internal noise and vibration of minivan markedly increased and it came out a booming noise which oppressed the human occupants' eardrums. The booming noise could make significant contribution to the human occupants' discomfort and fatigue [6]. This problem became more serious when the minivan transmission was at the 3th, 4th, or 5th gear. Moreover, this phenomenon was found to be not associated with the vehicle driving speed; there was also no such noise when the vehicle engine reversed through the same speed range during deceleration or when the transmission is in neutral.

Front-engine-rear-wheel-drive (FR) is the most common layout of minivans. It is found that almost all the manual-transmission FR minivans in Asia have the problem of internal booming noise during acceleration. Figure 1 shows the interior noise test results of some Asian mainstream brands minivans driving at the 4th speed.

It is illustrated in Figure 1 that, for the desirable case, the interior noise sound pressure level (SPL) rises linearly as the engine speed increases and human occupants do not feel any discomfort or something abnormal, but for Minivans 1# to 5#, the interior noise SPL are quite high during the engine speed range from 900 r/min to 2000 r/min. Also, it can be seen in Figure 2 that the 2nd order component contributes the most to the internal noise, the peak of 2nd order noise SPL appears during the engine speed range from 900 r/min

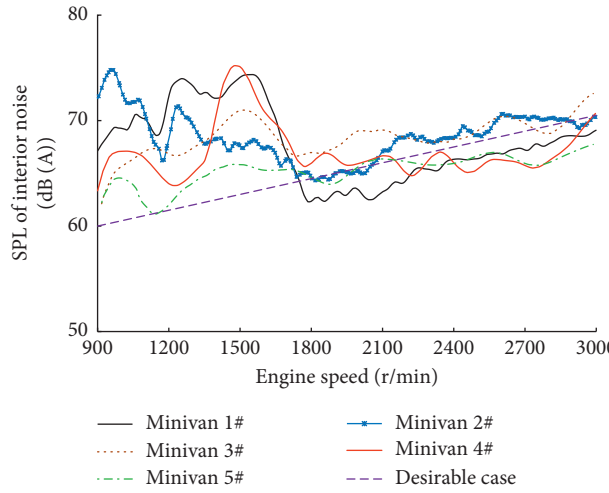

Figure 1: Interior noise during acceleration.

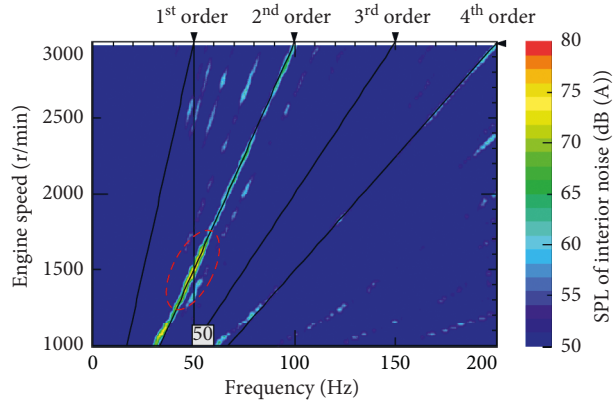

Figure 2: Colormap of minivan 4# interior noise during acceleration.

to 2000 r/min, and the frequency is around 50 Hz. This large-amplitude and low-frequency noise gives the occupants a strong feeling of booming.

Minivan 4# is one of the most popular minivans in China, due to its large amount of productions and customers, the noise issue is fully exposed and shown to be a common problem. It is a typical case of minivans: manual transmission (five forward gears and one reverse gear), 1.5 L displacement engine, and FR layout. In addition, the internal booming noise of Minivan 4# is very significant which is shown in Figure 1. So, in this study, Minivan 4# is set as the main research object to explore the generation mechanism and efficient approach to solve this problem.

3. Interior Booming Noise Generation Analyses

3.1. Analysis Method. The interior noise is the sum of the noises transmitted into vehicle cavity through multiple paths. As a typical structure-borne noise, the booming noise SPL can be expressed as formula (1) in the "Source-Path-Receiver" model:

$$p_k(\omega) = \sum_{i=1}^{n} \mathrm{FRF}_{ik}(\omega) \cdot F_i(\omega), \quad i = 1, 2, \ldots, n, \tag{1}$$

where $p_k(\omega)$ is the interior noise at point k, $\mathrm{FRF}_{ik}(\omega)$ is the frequency response function of structural paths i, $F_i(\omega)$ is the structural load at path location i, $\mathrm{FRF}_{ik}(\omega) * F_i(\omega)$ is the contribution of structural paths i, and n is the number of structural paths.

A car is a collection of multiple subsystems and the noise energy is transmitted to interior through multiple structures and spaces, such as tires, suspension, body, cavity, and so on (as shown in Figure 3). Therefore, the frequency response function for each transfer path can be expressed as

$$\mathrm{FRF}_{ik}(\omega) = \prod_{j=1}^{m} \mathrm{FRF}_{ikj}(\omega), \quad j = 1, 2, \ldots, m, \tag{2}$$

where $\mathrm{FRF}_{ikj}(\omega)$ is the frequency response function of structural paths i in subsystem j and m is the number of subsystems.

As the interaction in the multiple-subsystem collection is very complex, a Source-Path-Receiver-model-based approach is proposed to seek the main transfer paths and generation mechanism of minivan interior booming noise.

3.2. Experimental Transfer Path Analysis of Interior Booming Noise. To analyze the generation mechanism of minivan interior booming noise, the transfer paths by which the vibration energy enters vehicle cavity should firstly be identified. Experimental Transfer Path Analysis (TPA) provides an effective way to figure out this problem. Experimental TPA is a well-established technique for the estimation and ranking of individual low-frequency noise or vibration contributions via the different structural transmission paths from powertrain or wheel suspensions to the vehicle body [27–32].

In the analysis, the vehicle body is energized by n forces from attachment points of the powertrain and suspensions (as in equation (1)). Each force is composed of components in three directions (x-axis, y-axis, and z-axis, according to the vehicle dynamics coordinate system), and every force component contributes to interior noise through its transfer path. The individual path contribution to the sound pressure at point k from force acting at point i in direction q is given by

$$p_{kiq}(\omega) = \mathrm{FRF}_{kiq}(\omega) \cdot F_{ij}(\omega), \quad i = 1, 2, \ldots, n;\ \mathrm{q} = 1, 2, 3, \tag{3}$$

where p_{kiq} is the interior noise component, $\mathrm{FRF}_{kiq}(\omega)$ is the frequency response function from point i to point k, and $F_{iq}(\omega)$ is the force component.

When the sound pressure component on each transfer path is obtained, the contribution of each path to the interior noise can be calculated and the main transfer paths by which the vibration energy enters vehicle cavity can be identified.

For the FR minivan in this study, the scheme of the minivan internal booming noise TPA test is shown in Figure 4. The total number of the main attachment points is 20, including the engine mountings, the prop-shaft center support, front suspension, and rear suspension.

The test data acquisition hardware is Simcenter SCADAS Mobile, and the parameters of the sensors used in the TPA test are shown in Table 1. Matrix inversion method was used in the experimental TPA, and the acceleration sensors were installed at the active and passive ends of around attachment points, as shown in Figure 5(a), and the internal noise was collected by the sound pressure sensor in the middle of the rear seats (Figure 5(b)). The sampling frequency of microphone is 10240 Hz, and the sampling frequency of accelerometers is 1024 Hz. The acquisition time is 15 s, and the number of averages is 5.

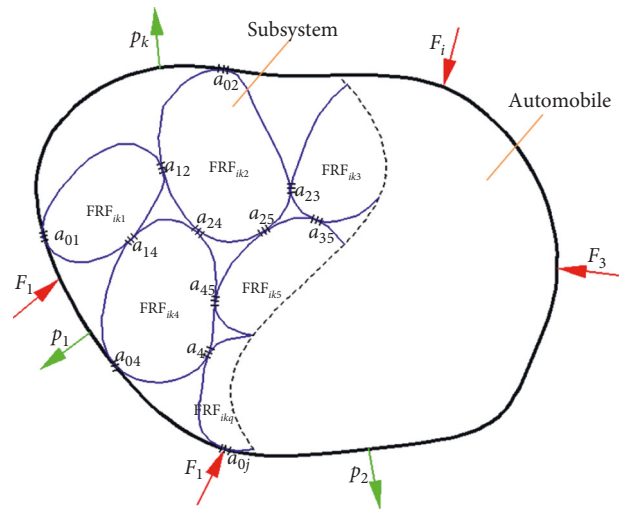

Figure 3: Sketch map of vibroacoustic energy flow in automobile.

The minivan internal noise TPA test was conducted on a four-wheel low-noise chassis dynamometer in semianechoic chamber, as shown in Figure 6. Figure 7 shows the results of minivan internal noise TPA results at 1500 r/min engine speed at the 4$^{\mathrm{th}}$ gear (when the booming noise occurred).

Eleven paths which make the largest contribution to the internal noise SPL are listed in Figure 7, and their locations and directions are displayed in Table 2. Figure 7(b) indicates that RSCS_L_Z and RSCS_R_Z in total contribute more than 70% to the minivan internal booming noise, so the rear suspension coil spring is identified as the main path to the internal booming noise.

3.3. Rear Suspension Dynamic Analysis. The rear suspension coil springs are the main transfer paths for the energy of interior booming noise, so the rear suspension dynamics is analyzed to explain how the vibration energy transfers in the rear suspension.

3.3.1. Operating Deflection Shapes of Rear Axle. Operational deflection shapes (ODSs) analysis provides an efficient way to obtain the forced motion of a structure and can be measured directly by relatively simple means. They provide useful information for understanding and evaluating the absolute dynamic behavior of a machine, component, or an entire structure. So, the rear axle dynamic was investigated based on ODS analysis to explore how the excitation energy generated as shown in Figure 8. The test was conducted in a semianechoic chamber shown in Figure 6.

Figure 4: Scheme of the minivan internal booming noise TPA test.

Table 1: Sensors used in the TPA test.

Sensor type	Microphone	Accelerometer
Model	PCB 378B02	PCB 356A02
Sensitivity	50 mV/Pa	10 mV/g
Frequency range	3.75 to 20000 Hz	1 to 5000 Hz
Mass loading	45.8 g	10.5 g

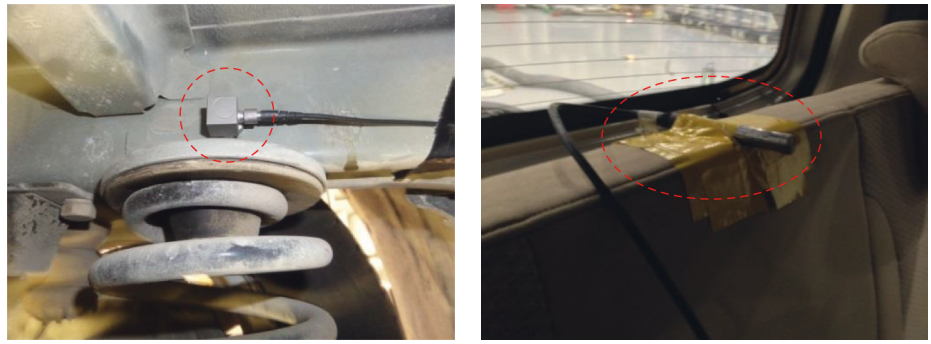

(a) (b)

Figure 5: Sensor installation of minivan internal noise TPA test. (a) Vibration acquisition. (b) Interior noise acquisition.

Figure 6: Minivan internal noise TPA test.

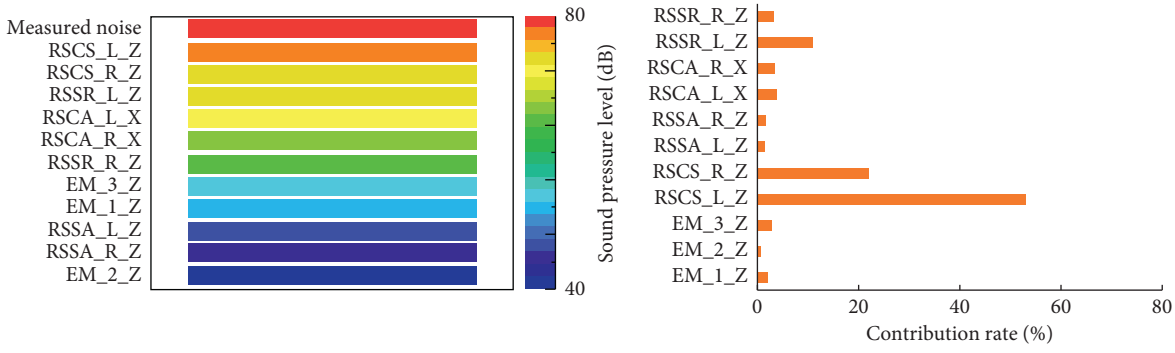

(a) (b)

Figure 7: Contributions of different transfer paths. (a) Ranking of contributions. (b) Percentages of contributions.

In the ODS test, the parameters of the accelerometers are shown in Table 3, and their locations are shown in Figure 9. The sampling frequency of accelerometers is 1024 Hz. The acquisition time is 15 s and the number of averages is 3.

Figure 10 shows the deflection amplitude changes over different engine speeds at the input shaft of the rear axle. The largest deflection shape appeared at the engine speed around 1500 r/min engine speed. At the engine speed around 1500 r/min, the deflection shape of rear axle is shown in Figure 11. It is illustrated that the largest deflection appears at the input shaft of the rear axle, the deflections near the drive shaft are very small, and the deflection shape is the rear axle pitching around the drive shaft (around the y axis of the vehicle).

3.3.2. Multibody Dynamics Analysis of Rear Suspension. To explore the cause of the rear suspension pitching, a multibody dynamics model of a combined system with

Table 2: Transfer paths description.

Abbreviation	Paths	Directions
EM_1_Z	Engine mounting (front-left)	z-axis
EM_2_Z	Engine mounting (front-right)	z-axis
EM_3_Z	Engine mounting (rear)	z-axis
RSCS_L_Z	Rear suspension coil spring (left)	z-axis
RSCS_R_Z	Rear suspension coil spring (right)	z-axis
RSSA_L_Z	Rear suspension shock absorber (left)	z-axis
RSSA_R_Z	Rear suspension shock absorber (right)	z-axis
RSCA_L_X	Rear suspension control arm (left)	x-axis
RSCA_R_X	Rear suspension control arm (right)	x-axis
RSSR_L_Z	Rear suspension strut rod (left)	z-axis
RSSR_R_Z	Rear suspension strut rod (right)	z-axis

Figure 8: Rear axle ODS test.

Table 3: Sensors used in test.

Sensor type	Accelerometer
Model	PCB 356A02
Sensitivity	10 mV/g
Frequency range	1 to 5000 Hz
Mass loading	10.5 g

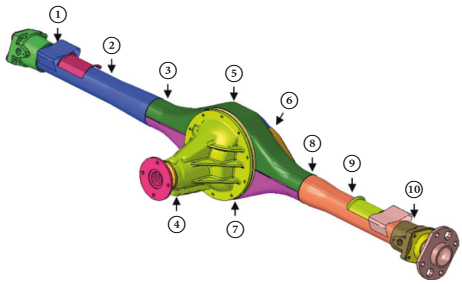

Figure 9: Sketch of the accelerometers' locations.

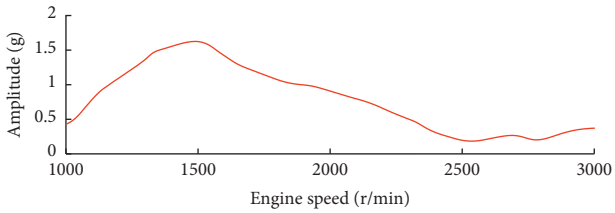

Figure 10: Deflection amplitude changes over different engine speeds.

propeller shaft, rear axle, and rear suspension is built as shown in Figure 12. The vehicle body is simplified as mass attached to the rear suspension.

The multibody dynamics model is driven by the rotational velocity at the in-put shaft of propeller shaft. The rotational velocity of the in-put shaft of propeller shaft is acquired in the torsional vibration test as shown in Figure 13. The parameters of the sensor used in the torsional vibration test are shown in Table 4. The sampling frequency of magnetoelectric sensor is 20000 Hz, the acquisition time is 15 s, and the number of averages is 5. Shown in Figure 14 is the rotational velocity fluctuation of propeller shaft input end.

When the engine speed is around 1500 r/min, the deflection of the rear axle is shown in Figure 15. The deflection amplitude is determined with the colors on the rear axle, the color scale of the deflection amplitude is on the left side of the picture, and the unit is millimeter. It is illustrated that the maximum displacement is concentrated in the input shaft of the rear axle, the displacements close to the drive shaft are small, and the rear axle is pitching around the drive shaft. In the results of the ODS analysis and multibody dynamics analysis, the deflection shapes of rear axle are the same, also the maximum displacements are all concentrated in the same location, so the multibody dynamics analysis result is consistent with the ODS test. It shows the drivetrain torsional vibration induces the rear axle pitching and finally causes the interior booming.

3.4. Drivetrain Torsional Vibration Analysis. To analyze the torsional vibration characteristic of minivan drivetrain, a lumped-parameter model is built. Lumped-parameter model is proved to be very efficient and reliable in driveline torsional vibration analysis [33–36].

The minivan driveline torsional vibration lumped-parameter model consists of a V4 engine, flywheel, clutch, transmission, propeller shaft, rear axle, rear wheel, and vehicle body. Details are shown in Figure 16, and the parameters are given in Table 5.

The vibration differential equations of the minivan drivetrain can be expressed as (4), and it also can be written in matrix form

$$\begin{cases} J_1\ddot{\theta}_1 + K_1(\theta_1 - \theta_2) = T_1, \\ J_2\ddot{\theta}_2 - K_1(\theta_1 - \theta_2) + K_2(\theta_2 - \theta_3) = T_2, \\ \quad \ddots \\ J_7\ddot{\theta}_7 - K_6(\theta_6 - \theta_7) + K_7(\theta_7 - \theta_8) + C_1\left(\dot{\theta}_7 - \dot{\theta}_8\right) = T_7, \\ \quad \ddots \\ J_{20}\ddot{\theta}_{20} - K_{18}(\theta_{19} - \theta_{20}) + K_{19}(\theta_{20} - \theta_{21}) \\ \quad + C_3\left(\dot{\theta}_{20} - \dot{\theta}_{21}\right) = T_{20}, \\ J_{21}\ddot{\theta}_{21} - K_{19}(\theta_{20} - \theta_{21}) - C_3\left(\dot{\theta}_{20} - \dot{\theta}_{21}\right) = T_{21}, \end{cases} \tag{4}$$

$$[J]\left\{\ddot{\theta}\right\} + [C]\left\{\dot{\theta}\right\} + [K]\{\theta\} = [T], \tag{5}$$

where $\{\theta\} = \text{diag}(\theta_1, \theta_2, \ldots, \theta_n)$ is the rotational angle vector, $[J] = \text{diag}(J_1, J_2, \ldots, J_m)$ is the rotational inertia matrix,

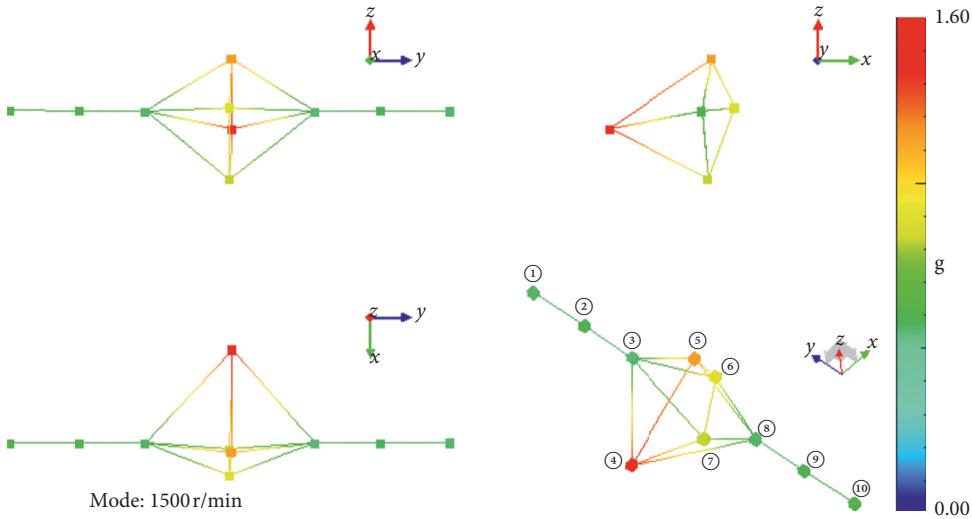

Figure 11: Operational deflection shape of rear axle at engine speed 1500 r/min.

Figure 12: Multibody model of minivan rear suspension.

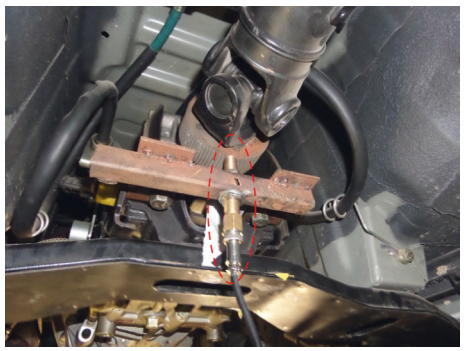

Figure 13: Torsional vibration measured at propeller shaft input end.

Table 4: Sensors used in torsional vibration test.

Sensor type	Magnetoelectric rotational velocity sensor
Model	KJT-CSHJ12
Frequency range	5~100000 Hz
Mass loading	52 g

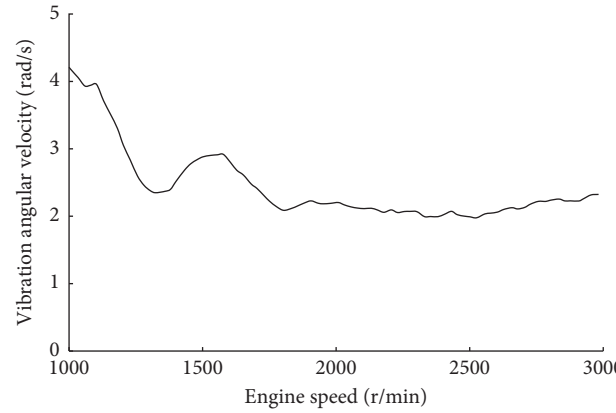

Figure 14: Angular velocity fluctuation of propeller shaft input end.

$[C] = \text{diag}(C_1, C_2, \ldots, C_k)$ is the damping matrix, $[K] = \text{diag}(K_1, K_2, \ldots, K_l)$ is the stiffness matrix, and $[T] = \text{diag}(T_1, T_2, \ldots, T_t)$ is the loads applied on the drivetrain.

Setting $[C]$ and $[T]$ in (5) to be zero, the modal frequency and mode shape of each order can be obtained from (4). Table 6 illustrates torsional vibration inherent characteristic of the minivan drivetrain. It shows that one of the drivetrain torsional modal frequencies is near 50 Hz.

Figure 17 shows the 5^{th} torsional vibration modal shape. In this mode, the largest vibration amplitudes are concentrated at the gearbox shafts, the propeller shafts and the rear axle shafts. The frequency of the 5^{th} torsional vibration mode is 50.5 Hz.

For V4 (four-cylinder) engines, every time the crankshaft rotates, two cylinders ignite, so the torsional vibration energy of V4 engines is concentrated in the frequency of their 2^{nd} order torsional vibration. For the rotational crankshaft, the frequency of the 1^{st} order and the 2^{nd} order torsional vibration could be calculated by

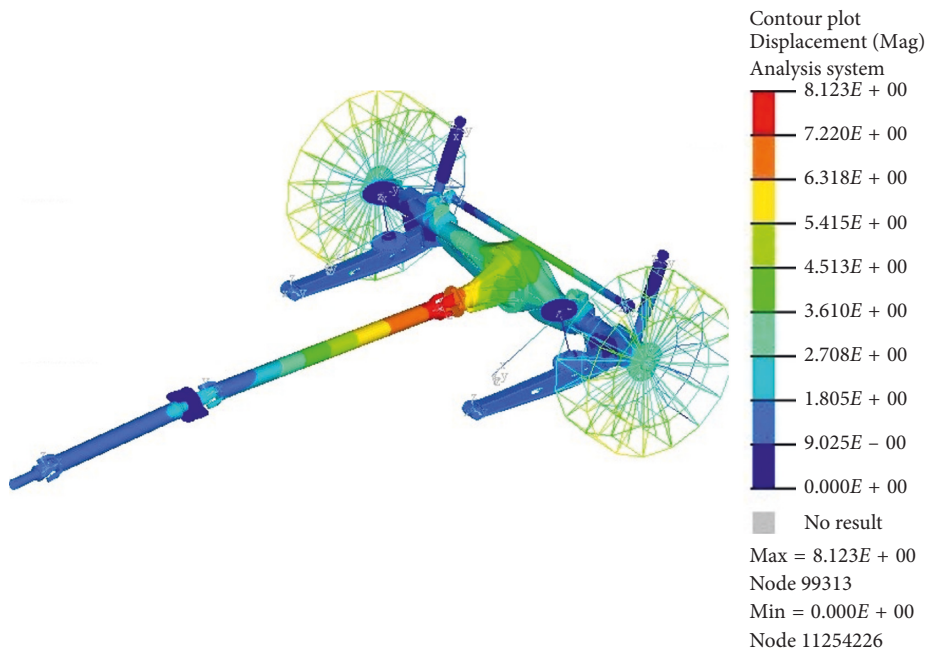

Figure 15: Pitching of rear axle.

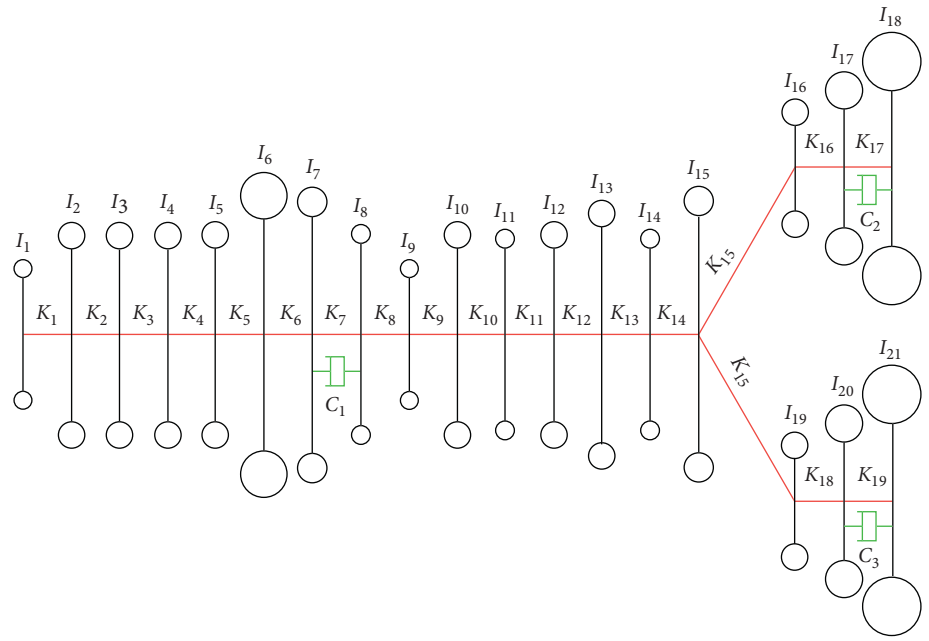

Figure 16: Lumped-parameter torsional vibration analysis model of minivan drivetrain.

$$\omega_{1st} = \frac{n_e}{60}, \tag{6}$$

$$\omega_{2nd} = \frac{n_e}{30}, \tag{7}$$

where ω_{1st} is the frequency of the 1st order torsional vibration, ω_{2nd} is the frequency of the 2nd order torsional vibration, and n_e is the engine rotation speed.

At 1500 r/min engine speed, according to equation (7), the frequency of the engine's 2nd order torsional vibration is 50 Hz. So, the 5th torsional vibration mode (50.5 Hz) could be excited by the 2nd order torsional vibration of the V4 engine at 1500 r/min engine speed (50 Hz); in other words, the drivetrain resonates at 1500 r/min engine speed.

To validate the delivery of vibration energy in the driveline, the torsional vibration load in Figure 14 is used to

Table 5: Lumped parameters of minivan drivetrain.

No.	Component name	Inertia (kg·mm^2)	No.	Component name	Stiffness (Nm/rad)
J_1	Engine free end	141	K_1	Engine free end	20883
J_2	Crankshaft first quarter	5386	K_2	Crankshaft first quarter	99891
J_3	Crankshaft second quarter	5512	K_3	Crankshaft second quarter	99891
J_4	Crankshaft third quarter	5512	K_4	Crankshaft third quarter	99891
J_5	Crankshaft fourth quarter	5421	K_5	Crankshaft fourth quarter	45363
J_6	Flywheel	70800	K_6	—	Rigid
J_7	Clutch drive end	20400	K_7	Clutch	344/2092
J_8	Clutch driven end	1130	K_8	—	Rigid
J_9	Gearbox input shaft	199	K_9	Gearbox input shaft	3155
J_{10}	Gearbox other	5076	K_{10}	Gearbox other	8574
J_{11}	Prop-shaft input part	966	K_{11}	Prop-shaft input part	32137
J_{12}	Prop-shaft first shaft	4334	K_{12}	Prop-shaft first shaft	58609
J_{13}	Prop-shaft second shaft	5632	K_{13}	Prop-shaft second shaft	27125
J_{14}	Rear axle input shaft	501	K_{14}	Rear axle input shaft	564
J_{15}	Differential	580	K_{15}	—	Rigid
J_{16}	Right axle shaft	3610	K_{16}	Right axle shaft	12992
J_{17}	Right wheel	430006	K_{17}	Right wheel	12447
J_{18}	1/2 vehicle body	58334153		—	
J_{19}	Left axle shaft	3654	K_{18}	Left axle shaft	11827
J_{20}	Left wheel	430006	K_{19}	Left wheel	12447
J_{21}	1/2 vehicle body	58334153		—	
No.	Component name	Damping (Nm s/rad)			
C_1	Clutch damping	200			
C_2	Right wheel damping	200000			
C_3	Left wheel damping	200000			

Table 6: Torsional vibration modal frequency.

Mode	Frequency (Hz)	Damping ratio
1	1.6	0.0205
2	6.9	0.0067
3	29.6	0.0002
4	37.7	0.0416
5	50.5	0.0114
6	209.5	0.0434
7	215.8	0.0980

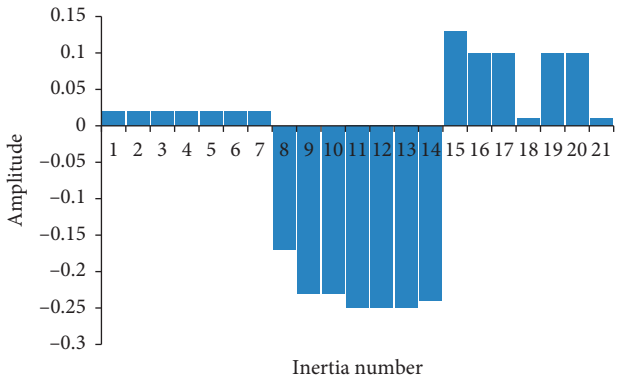

Figure 17: The 5th torsional vibration modal shape of the minivan drivetrain.

drive the drivetrain lumped-parameter torsional vibration analysis model, and the torsional vibration of the rear axle input shaft is acquired by drivetrain torsional vibration test. In the drivetrain torsional vibration test, the data acquisition hardware is Simcenter SCADAS Mobile, the parameters of the sensor are shown in Table 7, and Figure 18 shows the location of the rotational velocity sensor. The sampling frequency is 20000 Hz, the acquisition time is 15 s, and the number of averages is 5.

The lumped-parameter model simulation results and the torsional vibration test results are shown in Figure 19, and the simulation results are consistent with the test results. The drivetrain torsional vibration amplitude does not vary linearly with the engine speed, and it reaches a peak at the 1500 r/min engine speed, so a large amount of vibration energy is transferred to the rear suspension and finally leads to the interior booming noise.

4. Results and Discussion

4.1. Generation Mechanism Summary. With the Source-Path-Receiver model-based approach in Section 3, the flow of vibroacoustic energy from the engine to interior cavity is identified as shown in Figure 20. During the minivan acceleration, the 5th driveline torsional vibration mode is excited by the engine vibration at low speed around 1500 r/min. Then, the driveline torsional resonance carries a large amount of vibration energy to the rear suspension and causes a violent pitching vibration of the rear axle. The vibration energy of the rear axle pitching is transferred to the body and cavity and finally leads to the interior booming noise.

Table 7: Sensors used in drivetrain torsional vibration test.

Sensor type	Magnetoelectric rotational velocity sensor
Model	KJT-CSHJ12
Frequency range	5~100000 Hz
Mass loading	52 g

Figure 18: Rotational velocity sensor at the rear axle input shaft.

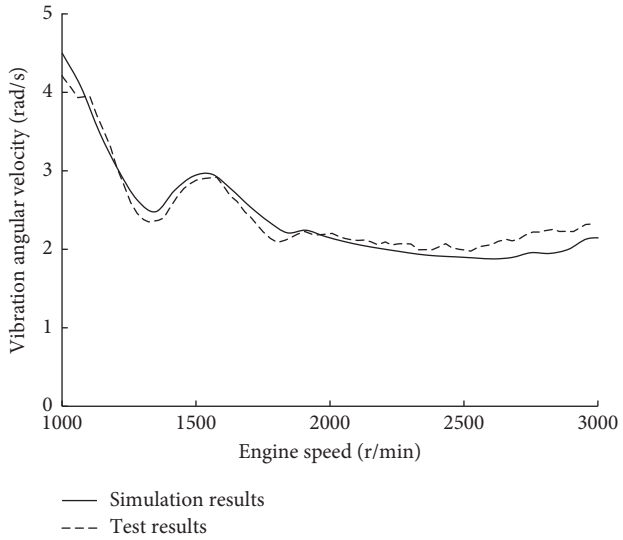

Figure 19: Comparison of drivetrain torsional vibration simulation and test results.

According to (1) and (2), the generation mechanism of minivan interior booming noise during acceleration can be mathematically expressed as

$$F_{\text{engine}}(\omega) * \left[\text{FRF}_{\text{driveline}}(\omega) * \text{FRF}_{\text{rearsuspension}}(\omega) * \text{FRF}_{\text{cavity\&body}}(\omega)\right] = p_{\text{booming}}(\omega), \tag{8}$$

where $F_{\text{engine}}(\omega)$ is the engine torsional vibration load, $\text{FRF}_{\text{driveline}}(\omega)$ is the frequency response function of driveline, $\text{FRF}_{\text{rearsuspension}}(\omega)$ is the frequency response function of rear suspension, $\text{FRF}_{\text{cavity\&body}}(\omega)$ is the frequency response function of body and cavity, and $p_{\text{booming}}(\omega)$ is the interior sound response.

4.2. Quantitative Validation

4.2.1. Engine Torsional Vibration Load. To quantify the engine torsional vibration load acting on the driveline, the flywheel angular velocity fluctuation is acquired during acceleration as shown in Figure 21, and the test results are shown in Figure 22.

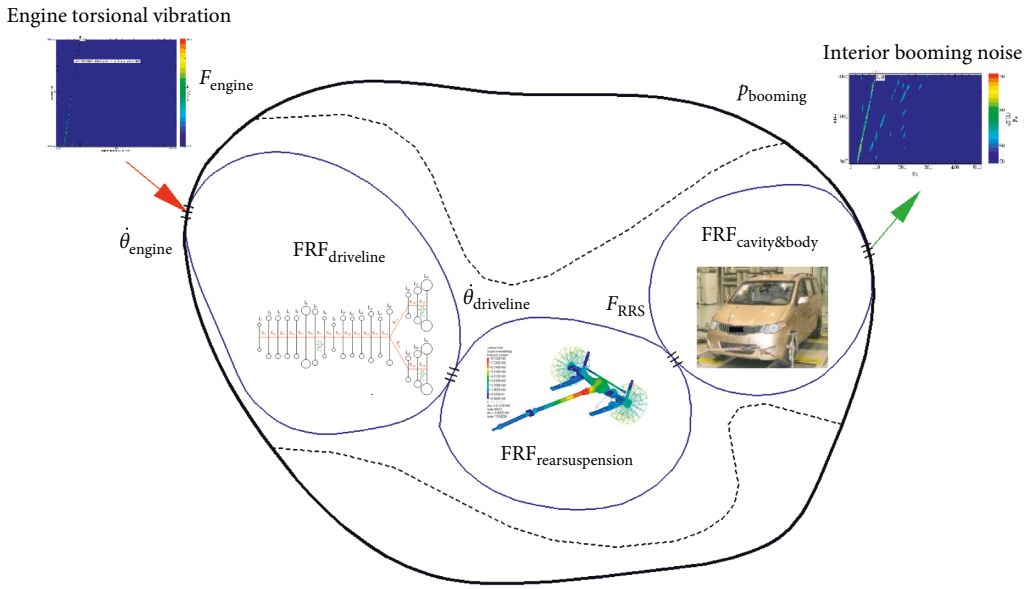

Figure 20: Mechanism of minivan interior booming noise.

Figure 21: Flywheel torsional vibration test.

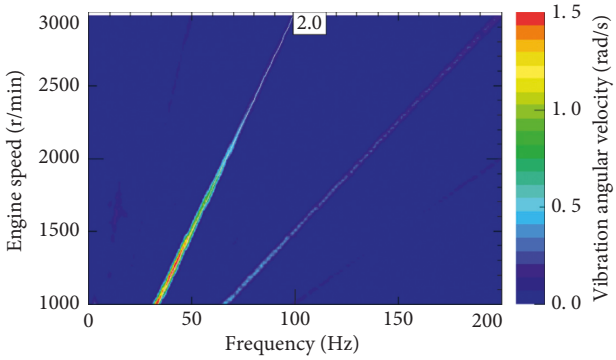

Figure 22: Engine flywheel torsional vibration angular velocity during acceleration.

It is illustrated in Figure 22 that the 2nd order vibration energy is the main component in the flywheel torsional vibration, and the fluctuation amplitude in the 2nd order is larger in low-frequency range and at low engine speed.

To obtain the input engine torsional vibration load at 1500 r/min engine speed, the angular velocity fluctuation is taken from Figure 22 and it is shown as Figure 23.

4.2.2. Frequency Response Function of Driveline. According to (4), the dynamic relation between flywheel to rear axle can be expressed as

$$\begin{cases} J_7\ddot{\theta}_7 - K_6(\theta_6 - \theta_7) + K_7(\theta_7 - \theta_8) + C_1\left(\dot{\theta}_7 - \dot{\theta}_8\right) = 0, \\ \ddots \\ J_{12}\ddot{\theta}_{12} - K_{11}(\theta_{11} - \theta_{12}) + K_{12}(\theta_{12} - \theta_{13}) = 0, \\ \ddots \\ J_{20}\ddot{\theta}_{20} - K_{18}(\theta_{19} - \theta_{20}) + K_{19}(\theta_{20} - \theta_{21}) \\ \quad + C_3\left(\dot{\theta}_{20} - \dot{\theta}_{21}\right) = 0, \\ J_{21}\ddot{\theta}_{21} - K_{19}(\theta_{20} - \theta_{21}) - C_3\left(\dot{\theta}_{20} - \dot{\theta}_{21}\right) = 0. \end{cases} \tag{9}$$

The frequency response function of the driveline can be expressed as

$$\mathrm{FRF}_{\mathrm{driveline}}(\omega) = \frac{\dot{\theta}_{14}(\omega)}{\dot{\theta}_6(\omega)}, \tag{10}$$

where $\dot{\theta}_6(\omega)$ is the angular velocity fluctuation of the flywheel and $\dot{\theta}_{14}(\omega)$ is the angular velocity fluctuation of the rear axle input shaft.

With the lumped parameters in Table 5, the frequency response function of the driveline can be calculated from (9) and (10), and $\mathrm{FRF}_{\mathrm{driveline}}(\omega)$ of the minivan is shown in Figure 24.

4.2.3. Frequency Response Function of Rear Suspension. The frequency response function of the rear suspension is the FRF from rear axle input shaft to the passive side of rear suspension. The $\mathrm{FRF}_{\mathrm{rearsuspension}}(\omega)$ can be calculated by the simulation of the minivan rear suspension multibody model in Figure 12, and the results are shown as Figure 25.

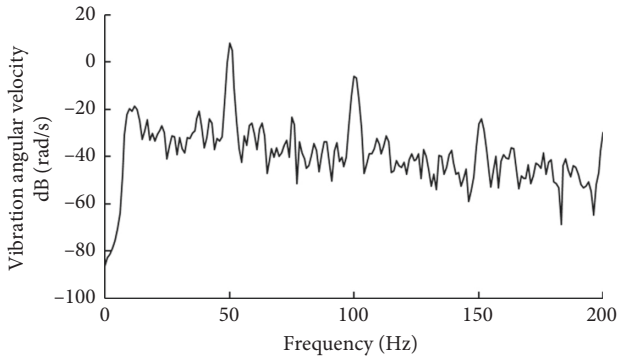

Figure 23: Engine flywheel torsional vibration angular velocity at 1500 r/min engine speed.

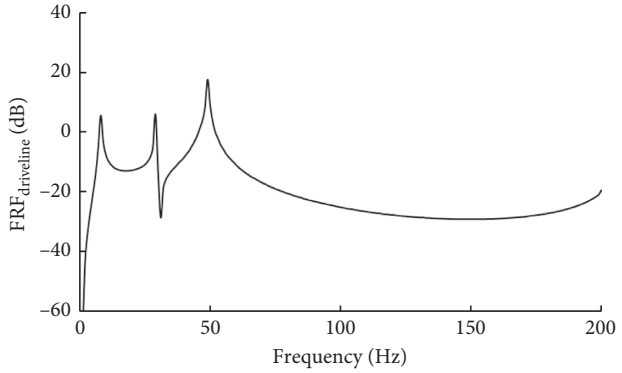

Figure 24: Frequency response function of driveline.

4.2.4. Frequency Response Function of Cavity and Body. With the experimental TPA in Section 3.2, the frequency response function from the passive side of the rear suspension to the interior noise can be taken out, and the $\mathrm{FRF}_{\mathrm{cavity\&body}}(\omega)$ is shown as Figure 26.

4.2.5. Comparison of Simulation and Test Results. Bringing the quantified $F_{\mathrm{engine}}(\omega)$, $\mathrm{FRF}_{\mathrm{driveline}}(\omega)$, $\mathrm{FRF}_{\mathrm{rearsuspension}}(\omega)$, and $\mathrm{FRF}_{\mathrm{cavity\&body}}(\omega)$ into (8), the interior noise at 1500 r/min engine speed can be calculated, and the comparison of simulation results and test results is shown in Figure 27.

It is illustrated in Figure 27 that the simulation-based interior noise SPL agrees with the test-based results in the low-frequency range. Especially at 50 Hz, the frequency and amplitude of the simulation-based interior noise SPL are very close to the test results. The energy through the identified path is the main contribution to interior booming noise of the minivan at 1500 r/min engine speed. The generation mechanism in 4.1 is validated. However, in the frequency range 100~200 Hz, the generation mechanism of the interior noise is different, and the noise energy is transferred into the cavity through other paths. Equation (6) is not applicative for the internal noise calculating in this frequency range, so the significant discrepancy appears between the interior noise test and simulation results in the frequency range 100~200 Hz.

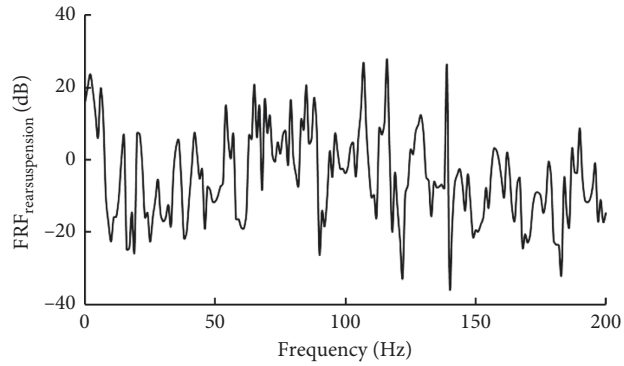

Figure 25: Frequency response function of rear suspension.

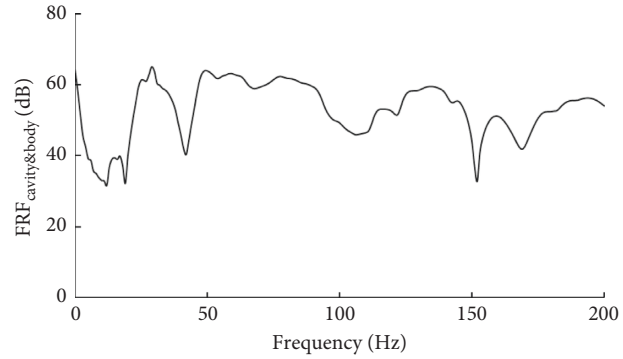

Figure 26: Frequency response function of cavity & body.

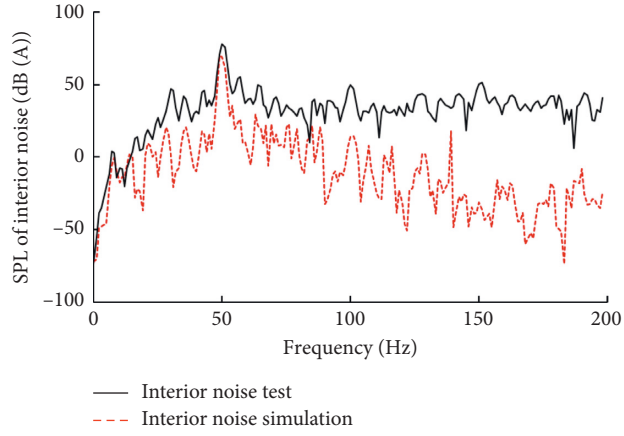

Figure 27: Comparison of simulation and test results.

4.3. Minivan Interior Booming Noise Reduction. According to the generation mechanism and (6), it is effective to reduce the interior booming noise $p_{\mathrm{booming}}(\omega)$ by decreasing $F_{\mathrm{engine}}(\omega)$, $\mathrm{FRF}_{\mathrm{driveline}}(\omega)$, $\mathrm{FRF}_{\mathrm{rearsuspension}}(\omega)$, or $\mathrm{FRF}_{\mathrm{cavity\&body}}(\omega)$ around 50 Hz. Since in real-world

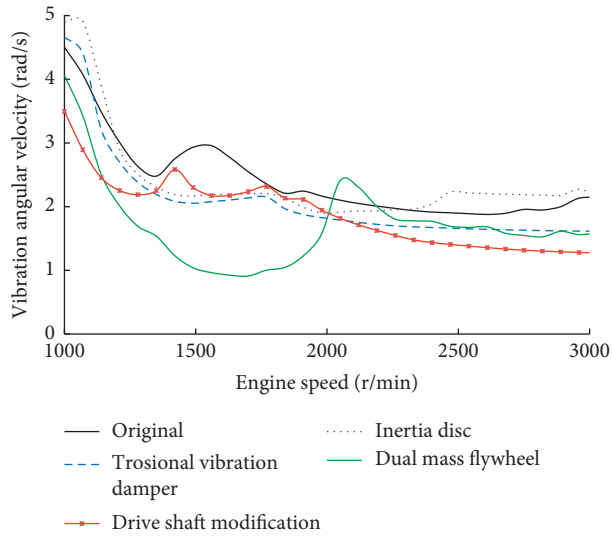

Figure 28: Driveline torsional vibration simulation results of drivetrain modifications.

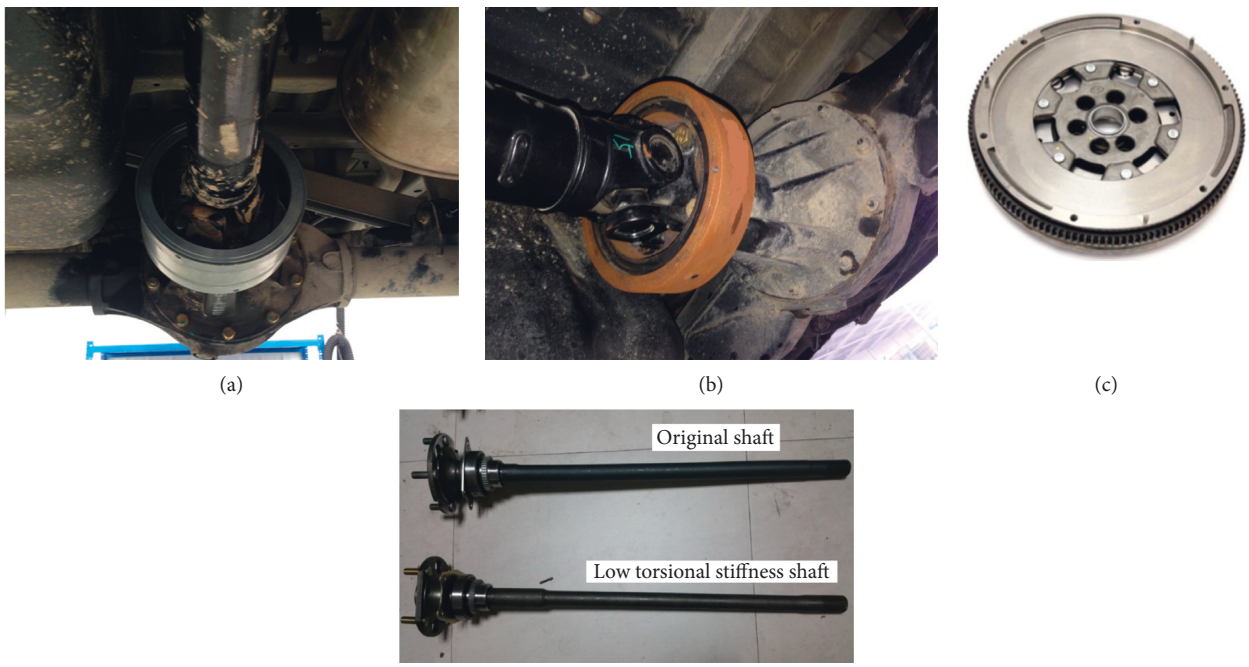

Figure 29: Drivetrain torsional vibration reductions. (a) Inertia disc. (b) Torsional vibration damper. (c) Dual mass flywheel. (d) Drive shaft modification.

engineering, when the car has already been put into production, it is very difficult to modify the engine, the optimizations focus on the frequency response function of the driveline, the rear suspension, and the vehicle body.

4.3.1. Driveline Modifications. To avoid the driveline resonance and suppress torsional vibration amplitude, the modifications of the driveline are as follows:

(a) Add an inertia disc at the propeller shaft

(b) Add a torsional vibration damper (TVD) at the propeller shaft

(c) Replace the single mass flywheel with dual mass flywheel (DMF)

(d) Reduce the torsional stiffness of the drive shafts

Bring the parameters of each modification to the model shown in Figure 16, respectively, and the simulation results of the driveline torsional vibration is shown in Figure 28.

It is illustrated in Figure 28 that the torsional vibration amplitude around 1500 r/min engine speed is reduced

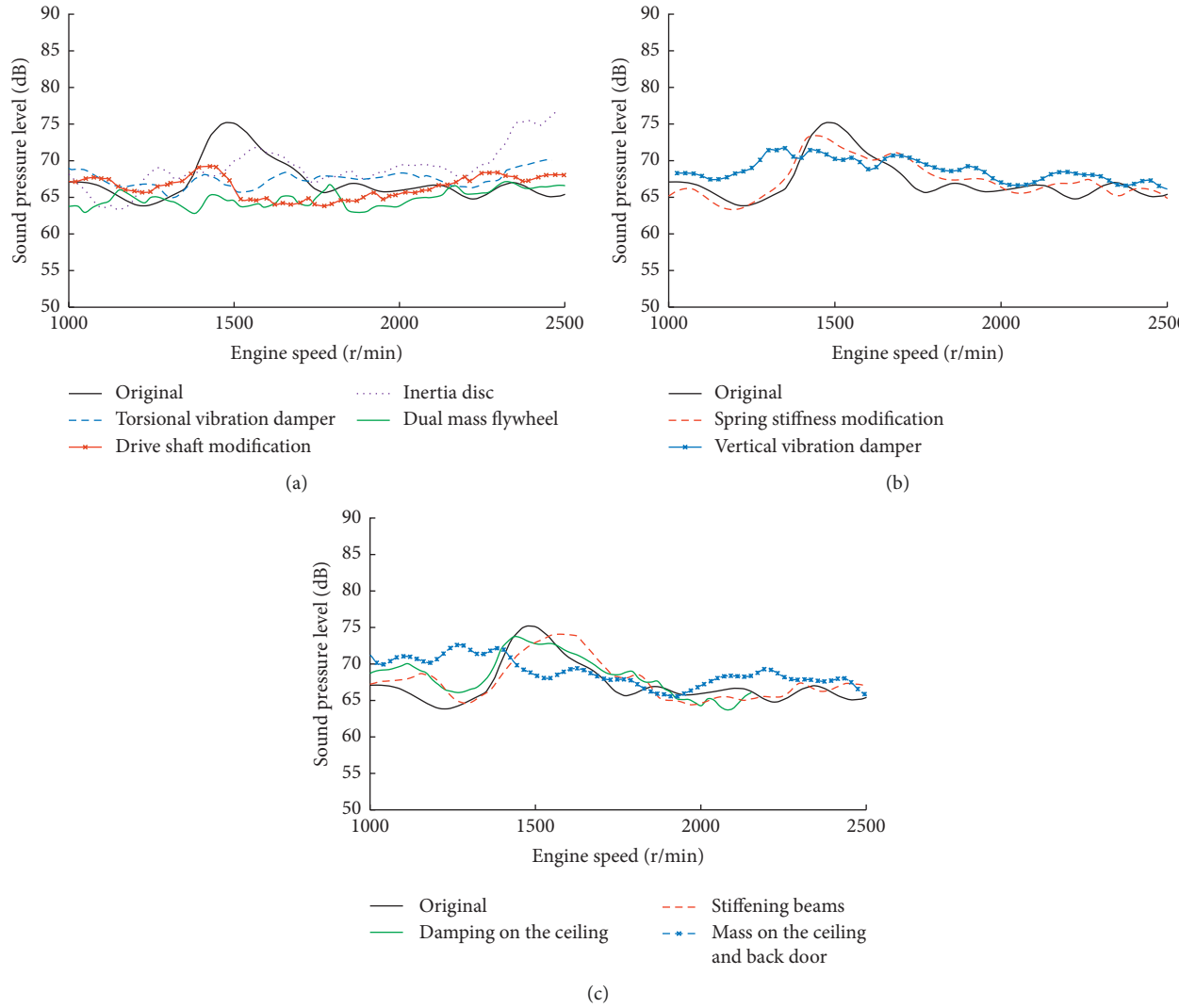

Figure 30: Internal noise experimental analysis of minivan with different modifications. (a) Driveline modifications. (b) Rear suspension modifications. (c) Vehicle body modifications.

obviously with the driveline modifications proposed above. The applications of the driveline modifications are shown in Figure 29, and the experimental results of the minivan interior noise during acceleration are shown in Figure 30.

4.3.2. Rear Suspension Modifications. To reduce the $\mathrm{FRF}_{\mathrm{rearsuspension}}(\omega)$, two modifications of the rear suspension are proposed:

(a) Reduce the suspension spring stiffness to improve the rear suspension vibration isolation around 50 Hz. To keep the handling stability performance, the maximum decrease is 10%. Shown in Figure 31 is the modified rear suspension spring.

(b) Add a vertical vibration damper to restrain the rear suspension pitching. The design frequency of the damper in the vertical direction is 50 Hz and the application of the damper is shown in Figure 32.

Figure 31: Suspension spring stiffness modification.

4.3.3. Vehicle Body Modifications. The FRF of vehicle body around 50 Hz is mainly influenced by large sheet metal parts; therefore, the ceiling and the back door is modified to reduce the minivan interior booming noise during acceleration. Shown in Figure 33 are the vehicle body modifications and

Figure 32: Axle pitching reduction with vertical vibration damper.

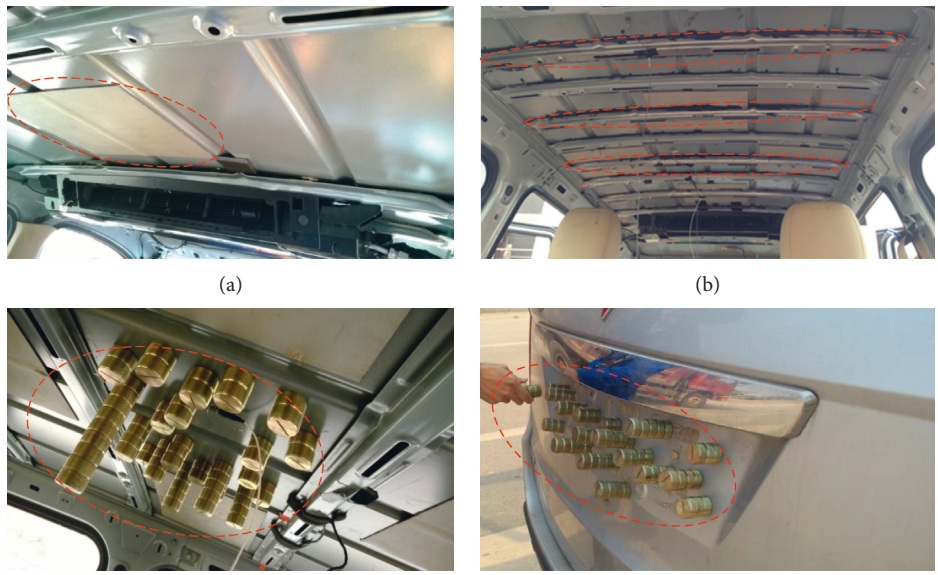

(a) (b) (c) (d)

Figure 33: Vehicle body modifications. (a) Damping on the ceiling. (b) Increasing the number of beams. (c) Mass on the ceiling. (d) Mass on the back door.

the experimental results of the minivan interior noise during acceleration are shown in Figure 30

4.3.4. Experimental Validation of the Noise Reduction Measures. The minivan interior noise during acceleration is recorded for each modification proposed in Sections 4.3.1–4.3.3. The experimental analysis results are shown as Figure 30

With the modifications to decrease the $\mathrm{FRF}_{\mathrm{driveline}}(\omega)$, the $\mathrm{FRF}_{\mathrm{rearsuspension}}(\omega)$, and the $\mathrm{FRF}_{\mathrm{cavity\&body}}(\omega)$, the interior booming noise is reduced around 1500 r/min engine speed during minivan acceleration. Among all the measures, DMF can observably reduce the interior noise around 1500 r/min engine speed without increasing the interior noise in other engine speed range. TVD at the propeller shaft, drive shaft stiffness modification, vertical vibration damper on rear axle, and mass on the ceiling and back door also make a good performance in interior booming noise reduction.

5. Conclusion

In this paper, a Source-Path-Receiver-Model-based approach is established to study the generation mechanism of minivan interior booming noise during acceleration. Also,

several modifications are proposed to reduce the minivan interior booming noise based on the generation mechanism. The following conclusions can be drawn from the results of this study:

(a) The generation mechanism of minivan interior booming noise during acceleration is identified. During the minivan acceleration, the 5^{th} driveline torsional vibration mode (50.5 Hz) is excited by the engine vibration at low speed around 1500 r/min. Then, the driveline torsional resonance carries a large amount of vibration energy to the rear suspension and causes a violent pitching vibration of the rear axle. The vibration energy of the rear axle pitching is transferred to the body and cavity and finally leads to the interior booming noise.

(b) The vibroacoustic energy in the transfer processes is quantitatively analyzed by the Source-Path-Receiver-Model-based approach. The identified generation mechanism is validated by the comparison of interior noise test results and quantitative simulation results. This approach also could be applied to study other similar complex automobile interior noise problems.

(c) Based on the generation mechanism, several modifications are proposed and applied to the interior booming noise reduction. With these modifications, the interior booming noise is reduced around 1500 r/min engine speed during minivan acceleration. The generation mechanism study and the proposed approach provide effective assistance with minivan interior booming noise reduction in engineering.

Data Availability

The data used to support the findings of this study are available from the corresponding author upon request.

Conflicts of Interest

The authors declare that there are no conflicts of interest regarding the publication of this paper.

Acknowledgments

This study was supported by the National Natural Science Foundation of China (grant number 51775451). The authors thank SGMW Automobile Co. Ltd and the China Automotive Technology & Research Center for supporting the completion of this work.

References

[1] J. Chen, "The Chinese automobile market and the strategies of european, American, Japanese, Korean and Chinese auto makers," *International Relations*, vol. 5, no. 5, pp. 241–257, 2017.

[2] R. Bartnik, M. Wilhelm, and T. Fujimoto, "Introduction to innovation in the East Asian automotive industry: exploring the interplay between product architectures, firm strategies, and national innovation systems," *Technovation*, vol. 70-71, pp. 1–6, 2018.

[3] J. L. Moraga-González, Z. Sándor, and M. R. Wildenbeest, "Consumer search and prices in the automobile market," *SSRN Electronic Journal*, vol. 7, no. 33, 2015.

[4] T. Wellmann, K. Govindswamy, and D. Tomazic, "Impact of the future fuel economy targets on powertrain, driveline and vehicle NVH development," *SAE International Journal of Vehicle Dynamics, Stability, and NVH*, vol. 1, no. 2, pp. 428–438, 2017.

[5] S.-K. Lee, "Objective evaluation of interior sound quality in passenger cars during acceleration," *Journal of Sound and Vibration*, vol. 310, no. 1-2, pp. 149–168, 2008.

[6] S.-H. Shin, J.-G. Ih, T. Hashimoto, and S. Hatano, "Sound quality evaluation of the booming sensation for passenger cars," *Applied Acoustics*, vol. 70, no. 2, pp. 309–320, 2009.

[7] H.-H. Lee and S.-K. Lee, "Objective evaluation of interior noise booming in a passenger car based on sound metrics and artificial neural networks," *Applied Ergonomics*, vol. 40, no. 5, pp. 860–869, 2009.

[8] D. J. Nefske, J. A. Wolf Jr., and L. J. Howell, "Structural-acoustic finite element analysis of the automobile passenger compartment: a review of current practice," *Journal of Sound and Vibration*, vol. 80, no. 2, pp. 247–266, 1982.

[9] S. Suzuki, S. Maruyama, and H. Ido, "Boundary element analysis of cavity noise problems with complicated boundary conditions," *Journal of Sound and Vibration*, vol. 130, no. 1, pp. 79–96, 1989.

[10] J. H. Park and S. K. Lee, "Identification of vehicle booming sound and its objective evaluation using psychoacoustic parameters," *International Journal of Vehicle Design*, vol. 58, no. 1, pp. 46–61, 2012.

[11] E. Yuksel, G. Kamci, and I. Basdogan, "Vibro-acoustic design optimization study to improve the sound pressure level inside the passenger cabin," *Journal of Vibration and Acoustics*, vol. 134, no. 6, Article ID 061017, 2012.

[12] A. Seifzadeh, A. Pietrzyk, P. Göransson, and R. Ramakrishnan, "Experimental investigation of coupling effects of passenger compartment and trunk of a car on coupled system natural frequencies using noise transfer function," *Applied Acoustics*, vol. 83, pp. 16–21, 2014.

[13] G. Accardo, P. Chiariotti, B. Cornelis et al., "Experimental acoustic modal analysis of an automotive cabin," *Sound and Vibration*, vol. 49, no. 5, pp. 10–18, 2015.

[14] L. Y. L. Ang, Y. K. Koh, and H. P. Lee, "Acoustic metamaterials: a potential for cabin noise control in automobiles and armored vehicles," *International Journal of Applied Mechanics*, vol. 8, no. 5, 2016.

[15] A. Oktav, G. Anlaş, and Ç. Yılmaz, "The effect of the folding rear-seat aperture in the acoustic response of a sedan car," *Proceedings of the Institution of Mechanical Engineers, Part D: Journal of Automobile Engineering*, vol. 231, no. 2, pp. 253–266, 2017.

[16] D. Siano and M. A. Panza, "Sound quality analysis of the powertrain booming noise in a diesel passenger car," *Energy Procedia*, vol. 126, pp. 971–978, 2017.

[17] T. Knechten, P. J. G. van der Linden, and M. Morariu, "Improved FRF acquisition method for vehicle body NVH analysis," *Sound and Vibration*, vol. 51, no. 4, pp. 8–13, 2017.

[18] T. Wellmann, K. Govindswamy, E. Braun, and K. Wolff, "Aspects of driveline integration for optimized vehicle NVH characteristics," *SAE Technical Paper Series*, vol. 1, no. 2246, 2007.

[19] K. J. Kim, H. J. Ju, Y. H. Lee et al., "Modeling and CAE simulation of chassis driveline test bench for vehicle NVH improvement," *Transactions of KSAE*, vol. 17, no. 1, pp. 114–119, 2009.

[20] T. Wellmann, K. Govindswamy, and G. Eisele, "Driveline boom interior noise prediction based on multi body simulation," *SAE Technical Paper Series*, vol. 1, no. 1556, 2011.

[21] G. Wu and W. Luan, "Review of dynamic research for NVH problems related to automotive driveline," *Journal of Mechanical Engineering*, vol. 49, no. 24, pp. 108–116, 2013.

[22] I. M. Khan, M. Datar, W. Sun, G. Festag, T. B. Juang, and N. Remisoski, "Multibody dynamics cosimulation for vehicle NVH response predictions," *SAE International Journal of Vehicle Dynamics, Stability, and NVH*, vol. 1, no. 2, pp. 131–136, 2017.

[23] H. Stoffels, "Balancing driveability, NVH, and fuel consumption on automotive powertrains using integrated simulation techniques," *Proceedings of the Institution of Mechanical Engineers, Part K: Journal of Multi-Body Dynamics*, vol. 231, no. 3, pp. 556–567, 2017.

[24] S. Lee, S. Lee, J. Back, and T. Shin, "A new method for active cancellation of engine order noise in a passenger car," *Applied Sciences-Basel*, vol. 8, no. 8, 2018.

[25] J. M. Mondot and B. Petersson, "Characterization of structure-borne sound sources: the source descriptor and the coupling function," *Journal of Sound and Vibration*, vol. 114, no. 3, pp. 507–518, 1987.

[26] R. A. Fulford and B. M. Gibbs, "Structure-borne sound power and source characterisation in multi-point-connected systems, part 1: case studies for assumed force distributions," *Journal of Sound and Vibration*, vol. 204, no. 4, pp. 659–677, 1997.

[27] G. Hur, "Isolation of micro-vibrations due to reaction wheel assembly using a source-path-receiver approach for quantitative requirements," *Journal of Vibration and Control*, vol. 25, no. 8, pp. 1424–1435, 2019.

[28] K.-S. Kim and Y. J. Kang, "Local stiffness control for reducing vehicle interior noise by using FRF-based synthesis method," *Journal of Mechanical Science and Technology*, vol. 25, no. 1, pp. 81–88, 2011.

[29] W. Li, "Transfer path analysis of effect of road surface excitation on vehicle ride comfort," *Journal of Jilin University (Engineering and Technology Edition)*, vol. 41, no. 5, pp. 1193–1198, 2011.

[30] Y. Cheng, H. Chunlin, and H. Meilong, "A method for identification of transfer path of abnormal interior sound caused by front-end accessory," *International Journal of Vehicle Noise and Vibration*, vol. 12, no. 4, pp. 331–345, 2016.

[31] J. Tatlow and M. Ballatore, "Road noise input identification for vehicle interior noise by multi-reference transfer path analysis," *Procedia Engineering*, vol. 199, pp. 3296–3301, 2017.

[32] E. Courteille and F. Mortier, "Experimental transfer path analysis in the diagnosis of engine mounting system for idle shake vibrations," in *Mechanika 2018. Proceedings of the 23rd International Scientific Conference*, pp. 28–31, Kaunas University of Technology, Kaunas, Lithuania, 2018.

[33] M. Menday and M. Ebrahimi, "The application of dynamic modelling using parametric design methods for an automotive driveline system," in *Multi-Body Dynamics: Monitoring and Simulation Techniques*, H. Rahnejat and R. Whalley, Eds., pp. 69–79, John Wiley and Sons Ltd., Hoboken, NJ, USA, 1997.

[34] A. Farshidianfar, H. Rahnejat, M. Ebrahimi, and M. Menday, "Low-frequency torsional vibration of vehicular driveline systems in shuffle," in *Multi-Body Dynamics: Monitoring and Simulation Techniques II*, H. Rahnejat, M. Ebrahimi, and R. Whalley, Eds., pp. 269–282, Wiley, Hoboken, NJ, USA, 2000.

[35] A. Farshidianfar, M. Ebrahimi, and H. Bartlett, "Hybrid modelling and simulation of the torsional vibration of vehicle driveline systems," *Proceedings of the Institution of Mechanical Engineers Part D-Journal of Automobile Engineering*, vol. 215, no. D2, pp. 217–229, 2001.

[36] J. Yang and T. C. Lim, "Influence of propeller shaft bending vibration on drivetrain gear dynamics," *International Journal of Automotive Technology*, vol. 16, no. 1, pp. 57–65, 2015.